Space Weather

RESEARCH ARTICLE
10.1029/2024SW003960

Substorm Identification With the WINDMI Magnetosphere - Ionosphere Nonlinear Physics Model

P. Adhya[1], **E. Spencer**[1], **and M. Kayode-Adeoye**[1]

[1]Electrical and Computer Engineering Department, University of South Alabama, Mobile, AL, USA

Key Points:

- The WINDMI model, a plasma physics-based nonlinear model, is used to analyze 10 years of substorm onsets obtained from the SuperMAG data set
- The WINDMI model, achieving a 32% substorm onset detection rate, is compared to auroral-image and SML-based rules used by various authors
- The influence of solar wind parameters in triggering substorm onsets through the energy loading/unloading mechanism is analyzed

Supporting Information:

Supporting Information may be found in the online version of this article.

Correspondence to:

P. Adhya,
purbiadhya@southalabama.edu;
purbi.adhya@gmail.com

Citation:

Adhya, P., Spencer, E., & Kayode-Adeoye, M. (2025). Substorm identification with the WINDMI magnetosphere - Ionosphere nonlinear physics model. *Space Weather*, *23*, e2024SW003960. https://doi.org/10.1029/2024SW003960

Received 17 APR 2024
Accepted 13 JAN 2025

Author Contributions:

Conceptualization: E. Spencer
Data curation: P. Adhya
Formal analysis: P. Adhya, E. Spencer, M. Kayode-Adeoye
Funding acquisition: E. Spencer
Investigation: P. Adhya, E. Spencer, M. Kayode-Adeoye
Methodology: P. Adhya, E. Spencer
Project administration: E. Spencer
Resources: P. Adhya, E. Spencer
Software: P. Adhya, E. Spencer
Supervision: E. Spencer
Validation: P. Adhya
Visualization: P. Adhya
Writing – original draft: P. Adhya

Abstract We investigate the applicability and performance of the plasma physics based WINDMI model to the analysis and identification of substorm onsets. There are several substorm onset criteria that have been developed into event lists, either from auroral observations or from auroral electrojet features. Five of these substorm onset lists are available at the SuperMAG website. We analyze these lists, aggregate them and use the WINDMI model to assess the identified events, emphasizing the loading/unloading mechanism in substorm dynamics. The WINDMI model employs eight differential equations utilizing solar wind data measured at L1 by the ACE satellite as input to generate outputs such as the magnetotail current, the ring current and the field-aligned currents (FACs). In particular, the WINDMI model current output I_1 represents the westward auroral electrojet, which is related to the substorm SML index. We analyze a decade of solar wind and substorm onset data from 1998 to 2007, encompassing 39,863 onsets. Our findings reveal a significant correlation, with WINDMI-derived enhancements in FAC coinciding with the identified substorm events approximately 32% of the time. This suggests that a substantial proportion of substorms may be attributed to solar wind driving that results in the loading and unloading of energy in the magnetotail.

Plain Language Summary The WINDMI model was designed to study the interactions between the solar wind–a stream of charged particles constantly flowing from the Sun–and the outermost part of Earth's atmosphere (magnetosphere and ionosphere). This study focuses on analyzing the model's effectiveness in predicting the onset of substorms, which are disturbances in Earth's magnetic field at high latitudes. We compared the model's results in analyzing substorms with studies based on observations of auroral images and ground measurements of magnetic fields at high latitudes, known as SML indices. As input to the model, we used solar wind speed and solar wind magnetic field strength, measured by the ACE spacecraft. From the outcomes of the model, we analyzed the behavior of an electric current in the region near the poles, called the Region 1 (R1) current. Our study found a strong correlation between the behavior of the R1 current and SML indices, demonstrating that the model successfully predicted many substorm onsets. We discovered that some substorms are more influenced by the solar wind than others, and the model could accurately predict these. However, we believe that there are other external factors that play a significant role in triggering substorms.

1. Introduction

Substorms are explosive events in the magnetosphere-ionosphere system that occur typically over a 20 min to 1–3 hr time scale (Baker et al., 1999). For decades, substorms have been identified by observing changes in auroral brightenings in the auroral oval (Akasofu, 1964; Feldstein et al., 1997). During the earliest days, substorms were studied by observing auroras, and they were interpreted as a large number of energetic particles entering the magnetosphere. Researchers investigated how solar wind energy is transmitted in the magnetosphere (Axford & Hines, 1961). Later, as solar wind data became available, studies on solar wind parameters and their combinations and their influence became more prominent (Akasofu, 1981). Recently, substorms have been identified using the SML index (P. T. Newell & Gjerloev, 2011a, 2011b), which is a generalization of the AL index (Davis & Sugiura, 1966).

Substorms exert significant effects on space weather by driving critical magnetospheric and ionospheric processes that impact both spaceborne and ground-based systems. The injection of energetic particles during substorms leads to surface charging and deep dielectric charging of spacecraft, increasing the risk of operational anomalies and potential catastrophic failures (Lanzerotti, 2001). These particle injections also intensify auroral activity (Baker et al., 1997), which induces ground-induced currents (GICs). These GICs pose substantial risks to power grid stability, particularly in high-latitude regions, where they can cause voltage fluctuations and, in severe

Writing – review & editing: P. Adhya, E. Spencer, M. Kayode-Adeoye

cases, widespread power outages (Kappenman, 2001). The localized and intense nature of substorm-induced GICs, which can be more damaging than those caused by geomagnetic storms, underscores the necessity for accurate forecasting and mitigation strategies to protect vulnerable technologies.

The events that occur during substorms can be divided into three phases. Firstly, there is a brightening of an equatorward auroral arc, followed by the arc expanding into the polar cap. In the end, the arc begins to dim, marking the conclusion of the substorm (Akasofu, 1964). These same events are also observed in the SML index. Whenever a substorm occurs, the SML index shows a sudden and sharp declination, with the values remaining low for around 20 min on average before starting to recover toward their pre-onset value. Based on the events observed in auroras and the signature seen in the SML index, substorms can be considered to have three phases (Kaufmann, 1987; R. L. McPherron, 1979). The growth phase is characterized by a slightly lower value in the SML index. The expansion phase is marked by the sudden intensification of auroral brightening and a sharp declination in the SML index. During the recovery phase, the auroral brightening dims down, and the SML index slowly increases toward a value that was present before the substorm occurred (Lyons, 1996).

The identification of the precise event triggering a substorm is a subject of ongoing research. However, authors such as Frey (Frey et al., 2004; Frey & Mende, 2006), Liou (2010), Newell (P. Newell & Gjerloev, 2011), Forsyth (Forsyth et al., 2015), and Ohtani (Ohtani & Gjerloev, 2020) employed various methods to detect substorm onsets. Frey and Liou utilized Polar UVI (Ultraviolet Imager) and IMAGE-FUV (Imager for Magnetopause-to-Aurora Global Exploration - Far Ultraviolet Imager) data, relying on auroral images for detection. Their method involved searching for poleward-spreading brightenings in the aurora lasting at least 20 min, with a minimum 30-min gap between successive onsets. Newell introduced the SML index, which exhibited an 0.86 correlation with auroral power, rendering it useful for substorm onset detection. According to Newell's rules, a substorm onset was identified based on specific criteria involving SML index differences. Forsyth's technique relied on percentile changes in the SML index, detecting substorm onsets when crossing certain thresholds; thus, Forsyth's technique can be used to identify both isolated and multi-onset substorms. Ohtani modified Newell's method particularly for isolated substorms, incorporating a sharp declination of the SML index and introducing a knee-like curvature condition, defined as the double rate of change of the SML index exceeding $1.5nT/\sec^2$.

There have been many models by several authors that use the energy and current dynamics of the magnetosphere-ionosphere system. Many of these models are based on the signatures of energy and current during substorms. The models by Morley et al. (2007), Beharrell et al. (2015), Ebihara and Tanaka (2017, 2023), Weimer (1994, 2001), Gjerloev and Hoffman (2002), Gordeev et al. (2017) approach substorm dynamics through various empirical and simulation-based methods. Morley et al. (2007) developed a synthetic AL index built on empirical relationships. This reduced-complexity model of magnetospheric energy storage, taken from Freeman and Morley (2004), is driven by solar wind input. Beharrell et al. (2015) focus on energetic electron injection and precipitation using onset timing data from the SuperMAG database, demonstrating the model's ability to predict precipitation hours after a substorm onset and accurately reproduce the morphology of spike events observed in ground-based data.

Ebihara and Tanaka (2017, 2023) explored field-aligned current (FAC) dynamics through global MHD simulations, emphasizing energy transfer processes during substorm expansion and identifying the sources of FACs. Weimer's models incorporate ionospheric electric potentials and convection patterns, utilizing empirical adjustments for realistic potentials and focusing on the time evolution of currents and electric fields following substorm onset (Weimer, 1994, 2001). Gjerloev and Hoffman (2002) construct a three-dimensional current system based on ionospheric conductances and convection electric fields, validating their model through comparisons with observed magnetic field perturbations. Gordeev et al. (2017) test global MHD models against statistical empirical data to evaluate how well they reproduce the global loading/unloading cycle of substorms.

In this paper, we demonstrate that the FAC often shows enhancement during substorms. Our goal through this paper is to establish a relationship between the FAC I_1 and the SML index and compare our results with the substorm lists provided by the five authors (Forsyth et al., 2015; Frey et al., 2004; Liou, 2010; P. Newell & Gjerloev, 2011; Ohtani & Gjerloev, 2020). Since WINDMI (solar WIND Magnetosphere Ionosphere) is only driven by data from the solar wind and does not include plasma instabilities, any enhancements in the FAC I_1 must result through the direct driving from the solar wind. This will help motivate further research on what really causes substorms.

In contrast to the previously described models, the WINDMI model provides a comprehensive, systems-based description of magnetotail current dynamics, particularly during isolated, stormtime, and periodic substorm events. It integrates the energy loading/unloading paradigm, focusing on the threshold exceedance of magnetotail plasma state variables to trigger substorm onset. While the previously referenced models emphasize different aspects and methodologies, such as empirical relationships, MHD simulations, and current system analyses, the WINDMI model offers a holistic, nonlinear approach that unifies these dynamics within a singular, physics-based framework.

The paper is organized as follows: the second section describes the data used in this study and the methodology adopted to condition the WINDMI model. Additionally, certain features like the trigger function were added to ensure the model's capability to detect substorms, and conditions were applied to the FAC I_1. The section also outlines how the results were measured against the merged substorm list, derived by combining onset lists from various authors. In this study, the five substorm lists were amalgamated to create a unified list with weighted values indicating the number of authors detecting a particular onset. The results obtained by running the model under these specific conditions are detailed in the results section.

2. Substorm Onset Detection by WINDMI

This section briefly describes the WINDMI model, the solar wind data and the parameters of the WINDMI model most significant in detecting substorm onsets. It outlines the trigger function introduced into the model, along with the specific conditions under which the model was run.

2.1. The WINDMI Model

The WINDMI model (Horton & Doxas, 1996, 1998) is a plasma-physics-based model that takes solar wind data as input. The model utilizes eight nonlinear differential equations to determine the energy flow through various components, including the magnetosphere tail, the neutral plasma sheet, the field lines connecting the tail of the magnetosphere and the ionosphere (Spencer et al., 2007). Several parameters, such as inductance, capacitance, and conductance of the magnetosphere tail and the ionosphere, are crucial in the model. The values of these parameters have been previously estimated (Mays et al., 2009; Spencer et al., 2007). The model has demonstrated success in predicting and analyzing geomagnetic storm signatures. The eight nonlinear differential equations encompass these parameters, contributing to a comprehensive understanding of the complex interactions within the Earth's magnetosphere-ionosphere system. For a full description of the model, please refer to Horton and Doxas (1996). The model is given by:

$$L\frac{dI}{dt} = V_{\mathrm{sw}}(t) - V + M\frac{dI_1}{dt} \tag{1}$$

$$C\frac{dV}{dt} = I - I_1 - I_{\mathrm{ps}} - \Sigma V \tag{2}$$

$$\frac{3}{2}\frac{dp}{dt} = \frac{\Sigma V^2}{\Omega_{\mathrm{cps}}} - u_0 p K_{\parallel}^{1/2}\theta(I - I_c) - \frac{pVA_{\mathrm{eff}}}{\Omega_{\mathrm{cps}}B_{\mathrm{tr}}L_y} - \frac{3p}{2\tau_E} \tag{3}$$

$$\frac{dK_{\parallel}}{dt} = I_{ps}V - \frac{K_{\parallel}}{\tau_{\parallel}} \tag{4}$$

$$L_I\frac{dI_1}{dt} = V - V_I + M\frac{dI}{dt} \tag{5}$$

$$C_I\frac{dV_I}{dt} = I_1 - I_2 - \Sigma_I V_I \tag{6}$$

$$L_2\frac{dI_2}{dt} = V_I - (R_{\mathrm{prc}} + R_{A2})I_2 \tag{7}$$

$$\frac{dW_{\mathrm{rc}}}{dt} = R_{\mathrm{prc}}I_2^2 + \frac{pVA_{\mathrm{eff}}}{B_{\mathrm{tr}}L_y} - \frac{W_{\mathrm{rc}}}{\tau_{\mathrm{rc}}} \tag{8}$$

where $V_{SW}(t)$ is the solar wind coupling function. L, C, and Σ are the inductance, capacitance, and conductances of the magnetosphere tail, and L_I, C_I, and Σ_I are the inductance, capacitance, and conductances of the ionosphere. Among the eight state variables, I denotes the magnetotail current, and I_1 denotes the Region 1 FAC.

Substorm initiation is caused by magnetic reconnection that occurs at the magnetosphere's tail. As a result of the reconnection, there is a current flow that occurs from the tail of the magnetosphere to the Region 1 part of the ionosphere. This increase in the flow of current should also be visible in the variation of the FAC. Thus, this enhancement should also be observable in the state variable I_1 of the WINDMI model.

2.2. Solar Wind Data

The solar wind data serving as an input to the WINDMI model, includes solar wind velocity (V_x) along the Sun-Earth line and the North-South component of the interplanetary magnetic field (B_z) data obtained from the ACE satellite. The product of these two parameters undergoes a filtering process, wherein the product is set to zero whenever B_z is positive. Subsequently, a small threshold voltage of 4 kV (represented as V_0 in Equation 9) is added to the product. This 4 kV addition represents a baseline adjustment introduced to better align the model with observed data. It accounts for base-level electric fields not captured by the simple vB_s coupling function alone, as identified in previous studies (Spencer et al., 2018), and helps match the model outputs with observations during periods of low solar wind driving. To account for the time it takes for solar wind to travel from the Lagrange point, where the satellite is located, to the nose of the magnetosphere, the data is time-shifted. This time shift is achieved by dividing the distance from the Lagrange point to the magnetosphere's nose by a 15-min running time-averaged value of the solar wind velocity where each point is shifted based on the average velocity, resulting in data with varying cadence. The data is then linearly interpolated onto a regular time series with each data point 1 min apart.

The rectified vB_s coupling function (Rostoker & Fälthammar, 1967) is computed using the formula:

$$vB_s = \begin{cases} V_0 + L_y|v_x||B_z|, & \text{if } B_z < 0, \\ V_0, & \text{otherwise.} \end{cases} \tag{9}$$

where V_0 is the small threshold voltage that is added to the coupling function vB_s, V_x is the solar wind velocity along the line joining the centers of the Earth and the Sun, and B_z is the North-South interplanetary magnetic field.

Figure 1 illustrates how the input for the WINDMI model is derived from solar wind data. The plot represents the calculation for a single day of ACE data, generating the input for the model. In Figure 1, Panel (a) displays the magnitude of the solar wind velocity toward Earth in km/sec throughout the day. Panel (b) illustrates the IMF in the north-south direction. To focus on periods potentially causing magnetic reconnection and initiating substorms, only intervals with a primarily southward-directed magnetic field were considered. Periods when the IMF was negative were either discarded or treated as zero during the coupling function calculation. Panel (c) demonstrates the resulting coupling function, representing the product of the solar wind velocity toward Earth and the IMF along the North-South direction when the IMF is directed southwards. Otherwise, it is set to zero, and a 4 kV threshold voltage is added.

2.3. Conditions of the WINDMI Model and Trigger

To detect substorm onsets, a trigger function is used in the WINDMI model (Horton & Doxas, 1996, 1998). The function is defined as a hyperbolic tangent function, chosen for its ability to provide a smooth, continuous transition from 0 to 1. The transition occurs when the magnetotail current, I, crosses the critical threshold I_c, indicative of substorm activity. The parameter ΔI, set to 0.1, controls the sharpness of this transition, effectively smoothing the onset detection to avoid abrupt discontinuities.

$$\theta(I - I_c) = \frac{1}{2}\left[1 + \tanh\left(\frac{I - I_c}{\Delta I}\right)\right] \tag{10}$$

Here, I_c represents a critical current above which energy unloading occurs, and δI controls the rate of transition. Substorms are known to occur under different magnetospheric conditions, such as size, shape, current levels, and energy content. Therefore, I_c is suspected to vary according to solar wind driving and the overall state of the

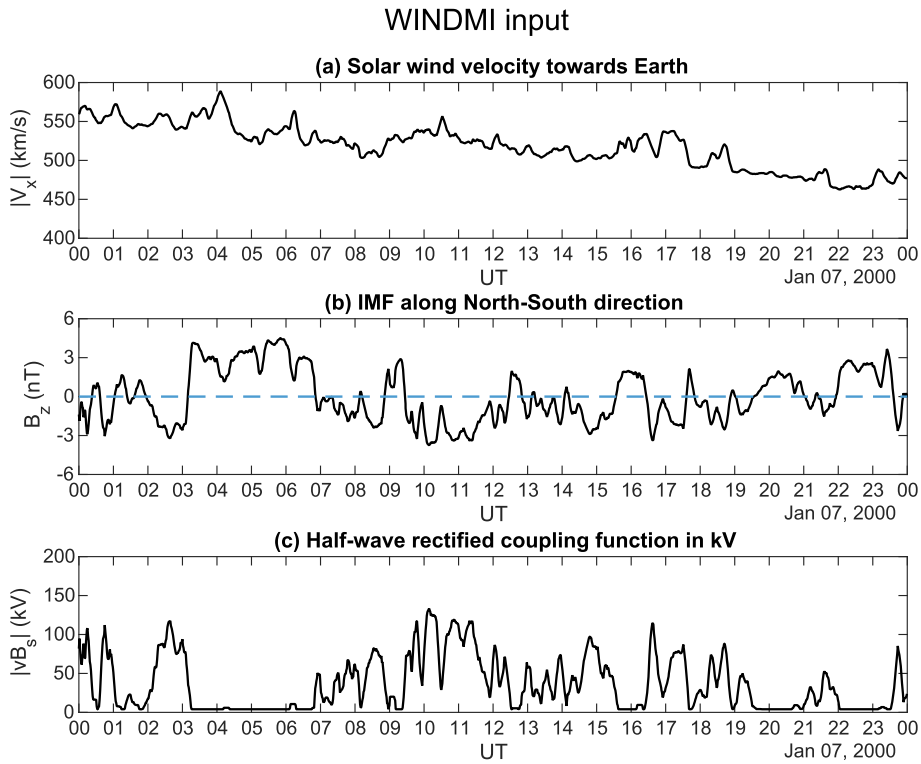

Figure 1. Illustration of the half-wave rectified vB_s coupling function used as input for the WINDMI model throughout a day. (a) Solar wind velocity along the Sun-Earth line. (b) IMF B_z indicating the North-South magnetic field (in GSM coordinate system), with the blue dashed line denoting the 0 value. (c) Rectified input obtained by multiplying solar wind velocity and southward-directed magnetic field, supplemented with a 4 kV threshold voltage.

magnetosphere, rather than remaining fixed. However, the exact time scale of I_c variations remains unclear and is being investigated as future work. In this study, daily values of I_c were chosen as a baseline to analyze the predictive capacity of the model in a first attempt. The overall character of the model (growth, expansion, and recovery phases) is strongly controlled by the first three equations.

For each day of substorm onset detection, the WINDMI model was run under two different conditions to identify substorm onsets. Initially, it was run with high critical current values set at 2×10^7 kA. This setup ensures that the trigger value always remains at 0. Subsequently, the model was run with critical current values set at the 70th percentile of the values obtained from the first run.

Figure 2 illustrates how the trigger function enhances the Region 1 current, emulating the triggering of a substorm and resulting in a sudden increase in FACs. The figure presents results from the WINDMI model for a day, with Panel (a) displaying the magnetotail current I in kA, Panel (b) showing the trigger function $\theta(I - I_c)$, and Panel (c) depicting the Region 1 current I_1 in kA, alongside the trigger function θ shaded in green. In Panel (a), which shows the magnetotail current, a blue dashed line represents the critical current I_c in kA. The panel demonstrates that the magnetotail current increases and crosses the threshold current.

To identify substorm onsets from the WINDMI model output, the trigger value was employed, and a threshold was set for the trigger. Whenever the trigger exceeded 0.1, we considered it as the onset time for substorms, as indicated by WINDMI.

2.4. Comparison With Other Models

To compare the results obtained from WINDMI and evaluate their consistency with substorm lists generated by Frey, Liou, Newell, Forsyth, and Ohtani, the triggering times of the WINDMI model were cross-referenced with a merged list of substorm onsets from these authors, using data from the SuperMAG website. The merged list was created by combining the onset times from the five lists provided by these authors; if two or more substorm onsets

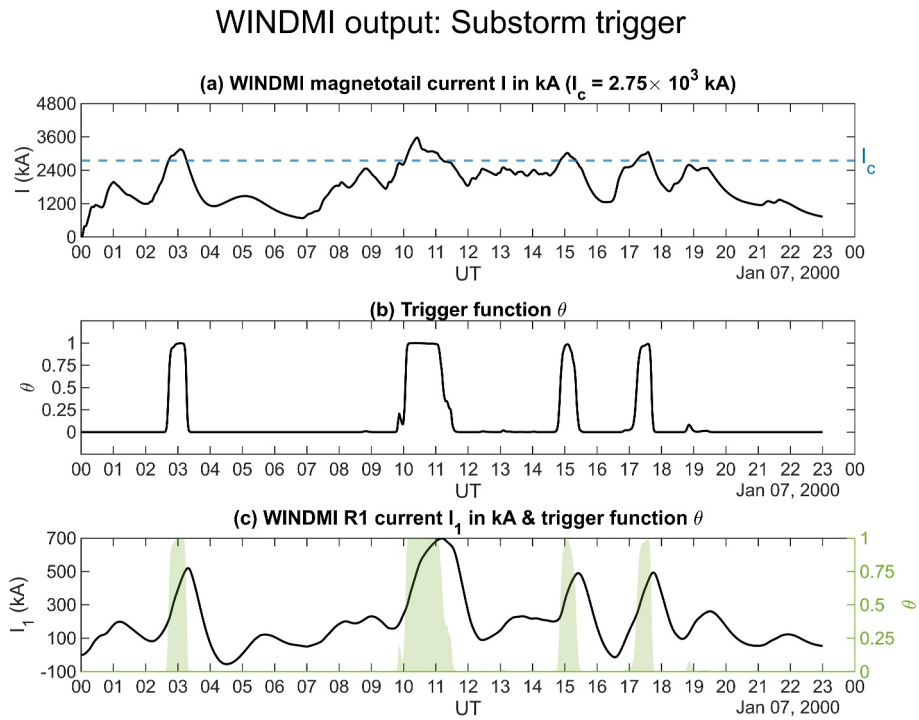

Figure 2. Figure: Illustration of the WINDMI model's trigger function $\theta(I - I_c)$ during a day. (a) Magnetotail current I and critical current I_c (blue dashed line). (b) Trigger function θ, increasing when I crosses I_c and decreasing when below. (c) Changes in Region 1 field-aligned current values, with green shading indicating periods of high θ values.

occurred within 15 min of each other, their onset times were averaged, and the coincident onset was considered a single substorm event. This process resulted in a total of 39,863 substorm onsets spanning 10 years. To determine the statistics of how often WINDMI's outputs align with this merged substorm list, a 30-min window centered around each substorm onset was considered: if any other substorm onset coincided with a triggering of the WINDMI model within this window, it was counted as a positive result.

The SML index (P. T. Newell & Gjerloev, 2011b) serves as a measure of the near-Earth magnetic field in the polar region. It is an enhancement over the AL index, which is the lower bound of the auroral electrojet index. After introduction of the SML index, Gjerloev's baseline elimination technique (Gjerloev, 2012) involved a three-step process for determining the baseline of a given station and component, incorporating a slowly varying offset or trend mainly attributed to the Earth's main field and a diurnal component largely associated with the solar quiet current system.

Figure 3 illustrates an example of merging three substorm onsets by different methods into one. The figure displays SML data during 7 January 2000, from 09:00 to 10:30 UT. The SML index value was initially slightly negative at around 09:00 UT, and it gradually decreased starting around 09:20 UT, suggesting the approximate growth phase. Around 09:30 UT, the SML value started to decrease rapidly, exhibiting multiple sudden declinations for about 30 min, indicating the expansion phase of the substorm. After 10:00 UT, the SML index value began to recover, signifying the recovery period of the substorm. Substorm onset is generally classified as the beginning of the expansion phase. Newell's substorm onset detection technique positions an onset whenever the index shows a sharp change in value $< -45nT/\text{sec}$, placing it just before the sharpest decline. On the other hand, Ohtani's identification method places the substorm onset around the inflection point of the curve, as it relies on identifying a knee-like nature in the SML curve. Forsyth, utilizing changes in percentage threshold, often detects substorm onsets before they are identified by other methods (Forsyth et al., 2015).

3. Results

The results section describes the input and output data for two selected days when the WINDMI model was run under the conditions outlined in the methodology section. The chosen dates, 17 March 1998, and 07 January 2000,

10.1029/2024SW003960

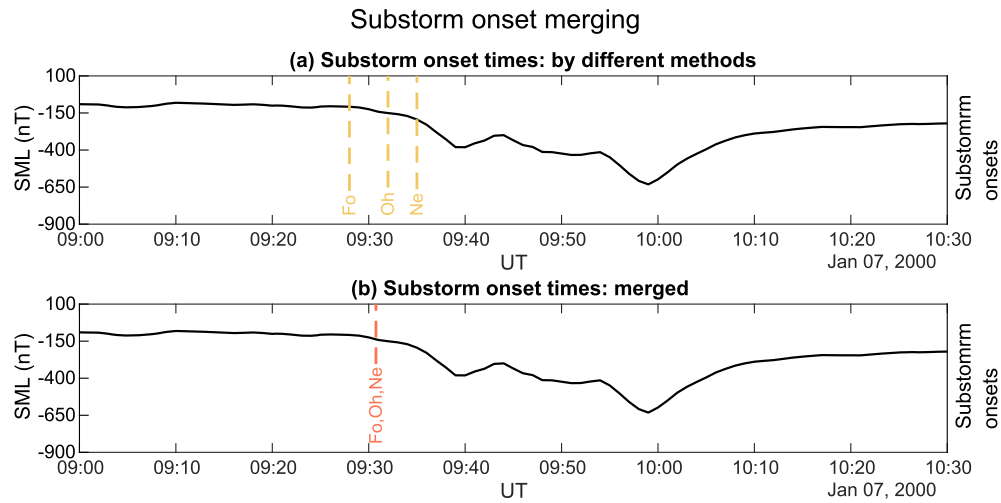

Figure 3. Example of merging substorm onset times obtained from different substorm lists from the SuperMAG website. The figure displays a 1.5-hr period. Both panels show the SML index in nT. Panel (a) features three dotted yellow vertical lines within approximately 5 min of each other, corresponding to Forsyth, Ohtani, and Newell (from left to right). Panel (b) illustrates the merged substorm onset as one dotted vertical line at the average of the three times shown in Panel (a).

were selected as representative examples of typical substorm occurrences observed during the 10-year period. These 2 days were specifically chosen for their characteristic substorm occurrence patterns: 17 March 1998, shows more isolated substorms, while 07 January 2000, features a higher number of closely spaced events in time. The results from the model during these days are presented alongside the substorm list produced by combining the substorm onset lists from the five different authors.

3.1. March 17, 1998

Figure 4 illustrates the WINDMI input and output during 17 March 1998. Panel (a) displays the solar wind input vB_s in kV throughout the day, including the IMF B_z in nT. The horizontal blue dashed line in the middle represents the zero magnetic field value. The shaded region above the dashed line represents northward, and the region below the line represents southward IMF, contributing to the coupling function vB_s. Panel (b) shows the magnetotail current I when the model is run with the input from panel (a). The critical current during the day, obtained from running the model with a high critical current ($I_c = 2 \times 10^7$ kA), is depicted as a blue dashed line. The resulting magnetotail current was used, and the 70th percentile of the current was employed for the second run of the model. The critical current is shown as a blue dashed line in the panel. The current is observed to have increased above the critical current seven times throughout the day. Panel (c) presents the resulting Region 1 FAC I_1 during the second run of the model. The periods when the trigger was on are indicated as regions shaded in green. When the trigger turns on, I_1 exhibits a knee-like bend in the current.

The knee-like shape is especially visible during the presumed substorm onsets near 01:30, 11, and 22 UT. The vertical dotted lines indicate the substorm onsets detected by the different authors mentioned previously. Throughout the day, it is observed that the enhancements in the R1 field-aligned and magnetotail currents and the knee-like bend in the R1 FAC, approximately representing substorm onsets, coincide with the onsets from the substorm list for the two substorms occurring near 01:30 and 22 UT. The enhancements roughly align with the onsets near 03 and 11 UT. Conversely, no enhancements in the R1 field-aligned and magnetotail currents were observed during the substorm onset near 07 UT. Incidentally, the substorm onset was detected by all four methods of substorm onset detection that were active during that period. Panel (d) displays the SML indices, and the vertical dashed lines with two-letter labels representing the authors' names associated with the methods used to detect the onsets show the substorm onset times. If more authors detected the same onset, the colors of the lines are reddish. An onset detected by only one method is shown in yellow. In the panel showing the R1 current, it is evident that the substorm onset at 22 UT is associated with the highest current enhancement and is also declared as a substorm onset by the four different techniques. Additionally, some enhancements in R1 current I_1 were not associated with any substorm occurrence; for example, the enhancement between 12 and 13 UT. During the two-

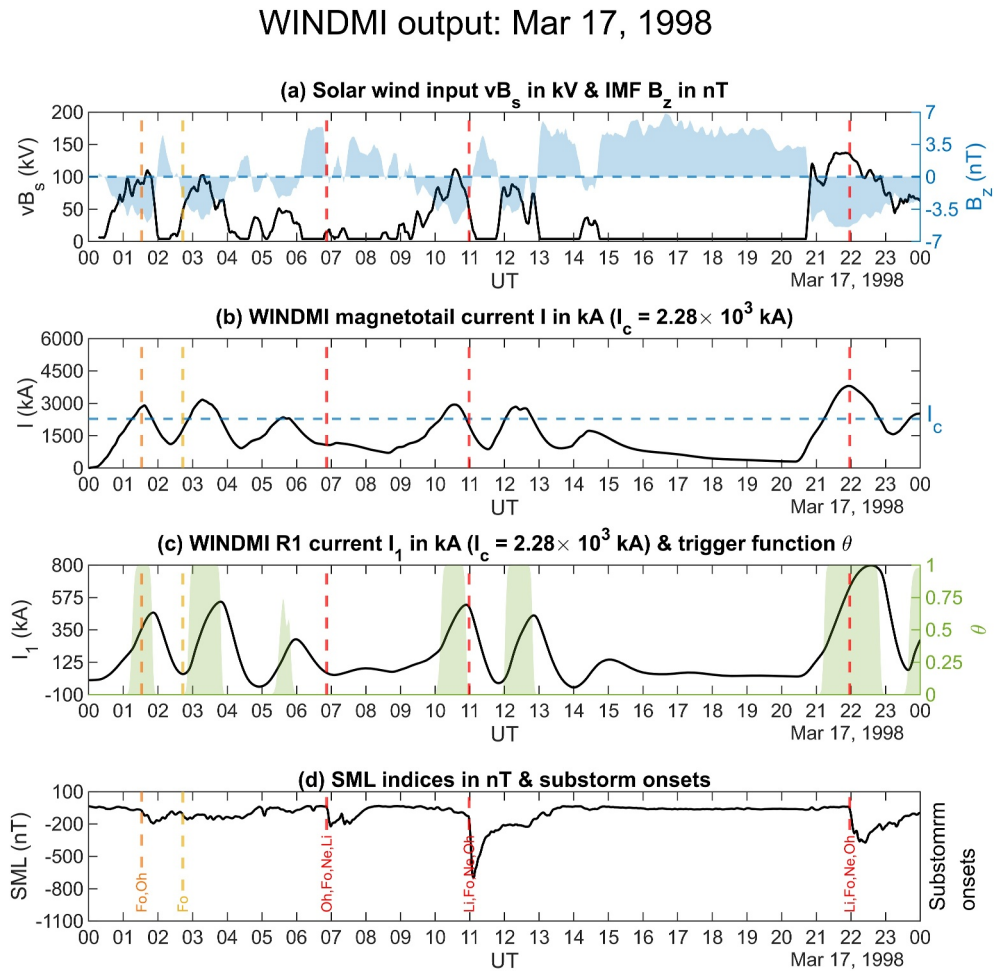

Figure 4. WINDMI output and SML index on 17 March 1998. (a) Solar wind input vB_s (black line) and IMF B_z (blue shades) with 0 nT reference line. (b) Magnetotail current I with critical threshold I_c (blue dashed line). (c) R1 current I_1 and trigger function θ in green. (d) SML indices with substorm onsets as dashed lines, color-coded by the number of concurring methods, and labeled by detecting authors' abbreviations.

hour period from 10 to 13 UT, there were two enhancements (one between 10 and 11 UT and another between 12 and 13 UT), but only one substorm signature was observed on the SML index.

3.2. January 07, 2000

Figure 5 displays WINDMI output during the day of 07 January 2000. On that day, Panel (a) illustrates that the solar wind input was sporadic and large for most of the day, with long periods when the IMF was notable and southward. Panels (b) and (c) depict the resulting magnetotail and Region 1 FAC derived from the differential equations of the WINDMI model. Panel (b) demonstrates that the magnetotail current I exceeded the critical threshold current I_c significantly four times, resulting in four trigger events seen in Panel (c). Panel (d) shows all the detected substorms during the day, displaying the SML index, indicating that several substorms were detected by Ohtani and Forsyth. However, not all methods agreed on the onset times of the substorms.

On the other hand, the R1 current shows four enhancements resulting from the trigger events. During the trigger events and corresponding current enhancements that occurred at 04, 16, and 18 UT, there were substorm signatures on SML indices. The event that occurred at 16 UT was detected by all four active methods during the period. The enhancements that occurred at 18 UT and 04 UT were detected by three and one methods, respectively. On the other hand, the model suggests there was a major enhancement that occurred between 11 and 12 UT when no substorm signature is seen on the SML index. Similarly, there was a major substorm that occurred near

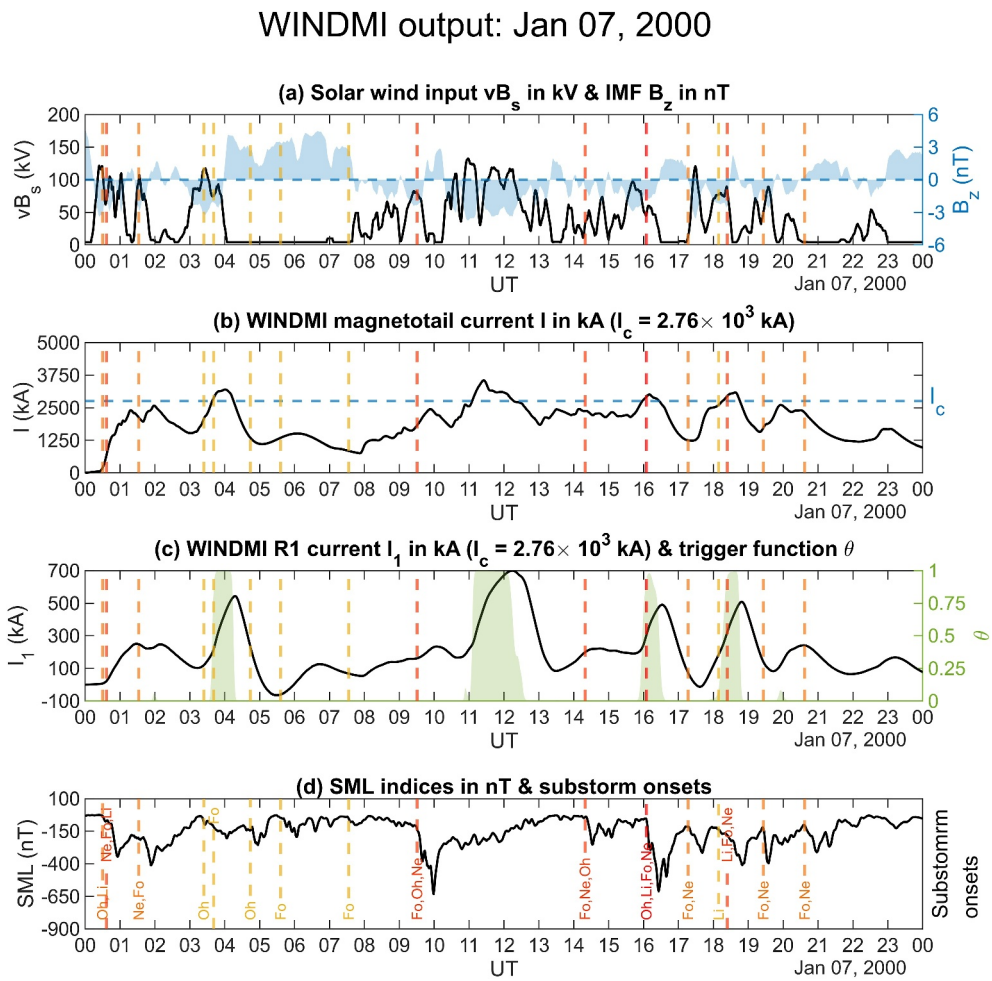

Figure 5. WINDMI output and SML index on 7 January 2000. (a) Solar wind input vB_s (black line) and IMF B_z (blue shades) with 0 nT reference line. (b) Magnetotail current I with critical threshold I_c (blue dashed line). (c) R1 current I_1 and trigger function θ in green. (d) SML indices with substorm onsets as dashed lines, color-coded by the number of concurring methods, and labeled by detecting authors' abbreviations.

09 UT that was detected by all four methods. There was a slight magnetotail current enhancement during the period, but the enhancement didn't surpass the critical current during the day and hence couldn't trigger a substorm. Similar events occurred during substorm events that were detected from the SML indices at 01, 02, 14, and 21 UT. During these events, there were enhancements in the magnetotail current but not enough to cause a trigger event. Additionally, there were slight enhancements near 08 UT or 23 UT when there were no substorms in proximity in time.

3.3. Comparison Results

Following the method described in Section 2.3 for the comparison of methods with the results from WINDMI, each substorm from the substorm list was compared with the WINDMI model output I_1 to analyze if there were trigger events associated with the onsets or not. For this comparison, 30-min windows centered around each onset were considered to check for trigger events. When merging onsets, onset times were combined if two onsets fell within a rolling 15-min window. Successive merging was performed to combine more than two substorm onsets. The resulting data is tabulated in Table 1, which shows that 32% of the time WINDMI is identifying substorm onsets detected by the five methods. Since only Frey or Liou's method was active at a single point in time during the chosen range of years, the two methods were combined into a single row representing the methods that used auroral images to detect substorm onsets. It can be observed from the data in the table that the triggered events by WINDMI mostly coincide with onsets detected by Newell and Forsyth and coincide least with the onsets detected

Table 1
Comparison Table for Other Methods Against WINDMI

Methods	WINDMI (detected)	WINDMI (not detected)	Total
Frey/Liou	1,611 (28%)	4,241 (72%)	5,852
Newell	7,328 (34%)	14,484 (66%)	21,812
Forsyth	8,692 (33%)	18,011 (67%)	26,703
Ohtani	2,561 (24%)	7,959 (76%)	10,520
Aggregated	12,884 (32%)	26,979 (68%)	39,863

by Ohtani and Frey/Liou. The coincidence of WINDMI's outputs with the five substorm detection methods, grouped into four categories—Frey/Liou, Newell, Forsyth, and Ohtani—shows agreement rates of 28%, 34%, 33%, and 24%, respectively. For the merged list (listed as aggregated in Table 1), WINDMI detected 32% of substorms, corresponding to 12,284 substorms out of a total of 39,863 substorms. Detailed data sets containing substorm onset information and the corresponding WINDMI triggers are provided Data sets 1 and 2 in Supporting Information S1.

Following the identification analysis, we calculated the false positive rate for the range of years during which the model was run to characterize substorms. This was done by considering all enhancements of θ. Using a similar approach to calculating true positive responses (where the model results matched the substorm lists), we defined 15-min windows around times when θ exceeded the threshold of 0.1. If no substorm was detected within the window, these incidents were considered false positives. Through this method, we found a total of 12,827 false positives out of 22,230 triggers from the aggregated list.

Additionally, a 90% confidence interval for the proportion of substorm onsets detected by WINDMI (using the aggregated list) was calculated to be between 31.93% and 32.71%, indicating a reliable level of confidence in the model's performance within the given data set.

Unfortunately, because our method does not employ a sliding window to detect the presence or absence of substorms within the window but instead uses an event-based matching or non-matching approach for substorm occurrences from both the model and the lists, we do not have a value for true negatives. Based on the true positive (TP = 12,884) and false negative (FN = 26,979) counts, along with the calculated false positive count (FP = 12,827), we determined the precision (the fraction of correct positive predictions), recall (the fraction of correct positive predictions), and F1 score (a balanced measure combining precision and recall) for the analysis:

$$Precision = \frac{TP}{TP + FP} = 0.5011$$

$$Recall = \frac{TP}{TP + FN} = 0.3232$$

$$F1\ score = \frac{TP}{TP + \frac{1}{2}(FP + FN)} = 0.393$$

4. Discussion

The analysis of substorms over a range of 10 years and their coincidence with WINDMI current enhancements demonstrates that using only solar wind data as input allows understanding the flow of energy and currents through the magnetosphere and ionosphere. The increased energy from solar wind manifests as enhanced current, often considered the result of substorm triggering within the magnetosphere. This enhanced current, along with other factors, significantly contributes to the sudden decrease in the SML index. The study aimed to analyze WINDMI results against the signatures on the SML index, represented by substorm onset lists from five different methods, and to measure WINDMI's performance in detecting substorm onsets. Approximately 32% of the substorm onsets identified by the WINDMI model coincided with substorm events listed in the combined list from the SuperMAG website, indicating a significant overlap and reinforcing the model's ability in capturing solar wind-driven substorms.

Recent studies, such as those by P. T. Newell and Liou (2011) and Liou et al. (2013), emphasize the significance of solar wind driving in substorm onset, showing a consistent need for an energy-loading phase characterized by an increased southward IMF component and heightened solar wind velocity, which drives energy into the magnetosphere (P. T. Newell & Liou, 2011). This aligns with the WINDMI model's approach, which uses solar wind parameters to understand substorm triggering.

However, the triggering mechanism remains a topic of debate. While some studies support the notion of a northward turning of the IMF prior to substorm onset (Lyons, 1996; R. McPherron et al., 1986), others argue that substorms are inherently driven by internal magnetospheric processes, with solar wind conditions playing a supportive but not necessarily triggering role (Johnson & Wing, 2014; Morley et al., 2009). The WINDMI model aligns with the idea that internal processes, such as the buildup of energy in the magnetotail, are crucial for substorm initiation. The model's focus on energy dynamics centers around the energy loading/unloading paradigm, positing that substorm onset occurs when the stored energy in the magnetotail exceeds a critical threshold, leading to a rapid release of energy. This perspective is supported by studies like Shukhtina et al. (2005) and Morley and Freeman (2007), who highlight the importance of energy storage in the magnetotail and its sudden release during substorms.

Moreover, comparisons of the current dynamics obtained by WINDMI in this work with the Weimer (1994) model reveal significant overlap in research methodology and certain aspects of the outputs. The Weimer model shows that FACs increase by about 420 kA during substorms, with dayside currents rising linearly an hour before onset and nightside currents increasing 20–30 min before onset. After onset, nightside currents and the SML index align with the Weimer model, which describes current increases using a capacitive-resistive circuit (Forsyth et al., 2018; Weimer, 1994). The WINDMI model captures key aspects of these dynamics, providing a complementary approach to understanding substorm behavior.

To emulate the triggering of substorms at the magnetotail resulting in an increase and sudden release of energy at the magnetotail, the $\theta(I - I_c)$ function was added to the WINDMI equations. This addition replicates the conditions during substorms and mimics the knee-like behavior in the SML index that occurs during these events (Ohtani & Gjerloev, 2020). The 15-min window used to measure the results of WINDMI against the methods followed the window used to merge substorm onsets if they occurred within the same timeframe. This window was chosen to account for potential uncertainties in substorm onset times, with the uncertainty window set to 15 min.

Moreover, the values of I_c fixed for each day could be considered a variable parameter representing the threshold of energy and current that should be surpassed during the triggering of substorms. As the value was kept fixed, the magnetotail current often approached but didn't surpass it, failing to trigger substorms. Keeping I_c variable and finding its dependence on other parameters is the main focus in the future, with ongoing studies on how the values of parameters affect the model.

Many WINDMI enhancements didn't transcend into substorms even though there was clear indication of energy storage in the magnetotail. This can be addressed in future by making the critical current I_c a varying parameter in time. Several substorm onset times were also seen to shift initiation times compared to the substorm onset list by the authors. This might also result from a variable threshold; for example, if the energy storage threshold was lower during the substorm on 07 January 2000, around 10 UT, it could show a different outcome if the threshold was low during that period. The slight enhancement in the current during that time could manifest into a substorm, contributing to the intense nature and prolonged recovery phase of the substorm.

In conclusion, while the WINDMI model effectively captures solar wind-driven substorms, the study highlights the importance of both external solar wind conditions and internal magnetospheric processes in triggering substorms. Future work will focus on refining the model by making parameters like I_c variable in time and understanding their dependencies, thereby enhancing the model's predictive capability.

5. Summary and Conclusions

In this work, we are trying to refine our approach to detect substorm onsets using the nonlinear physics model WINDMI, which consists of eight differential equations describing the energy flow through the magnetosphere-ionosphere system. Our goal in this paper was to utilize this model to determine onsets based on the flow of FACs, which often exhibit significant variations and enhancements during substorms. To achieve this, we used the WINDMI variables $\theta(I - I_c)$ and I_1, designed to identify specific enhancements in Region 1 FAC resulting from the increased magnetotail current triggered by substorms. These enhancements were then compared against a substorm list obtained by merging lists from five different authors, employing a 15-min window for merging. Similarly, 15-min windows were used to verify whether onsets detected by WINDMI were also identified by other

detection methods. The resulting statistics, as shown in Table 1, suggest that positive results from WINDMI can be associated with substorms significantly influenced by solar wind.

The two selected days discussed in the paper, namely 17 March 1998, and 07 January 2000, reveal frequent enhancements in the Region 1 FAC (I_1) during substorms, as indicated by the substorm lists. These enhancements are triggered by the activation of the θ function. The critical current (I_c) was held constant from day-to-day and optimized to a level where the trigger would activate only when the magnetotail current value exceeded a specific daily average. The primary reason the model struggles to predict substorms are that it can only do so when substorms are solely driven by solar wind and can be attributable to the dynamics of energy loading and unloading. Additionally, the critical current value needs to be somewhat variable to enable the enhancements corresponding to onset that generate substorms.

The final statistics demonstrate that the WINDMI model can predict substorms 32% of the time when provided with solar wind data. This capability proves valuable for approximating substorm times, estimating substorm intensities, and increases our understanding of substorm occurrences primarily attributable to the energy loading - unloading mechanism.

Data Availability Statement

The solar wind data utilized in this study were acquired from https://cdaweb.gsfc.nasa.gov/index.html. The substorm lists used were obtained from https://supermag.jhuapl.edu/substorms/. MATLAB 2023b was the software employed to execute the WINDMI codes, with the Simulink library being specifically utilized to model the WINDMI equations. All codes utilized and data sets generated in this study are available for download at the following link: https://zenodo.org/records/14607257 (Adhya, 2025).

For readers interested in replicating aspects of this study, we recommend using the provided code for optimal accuracy and reproducibility. It is also worth noting that the WINDMI model is accessible via the NASA CCMC platform. The CCMC version is designed for general use and operates with a fixed set of WINDMI parameters that differ from those used in our analysis. Among the outputs available in the CCMC version, the most comparable parameter to the R1 field-aligned current (I_1) is the AL index, which is derived by scaling I_1 by a constant factor. Although the CCMC version includes a substorm trigger function, it does not explicitly present this variable in its outputs, making it less practical for directly identifying substorm onsets. Additionally, we employed a variable time delay for the propagation of solar wind parameters from the ACE satellite to the nose of the magnetosphere, based on the solar wind velocity along the Sun-Earth line (V_x). In comparison, the CCMC version treats this delay as a constant.

Acknowledgments

The authors express their gratitude to various contributors for their substorm timing lists, including the SOPHIE technique by Forsyth et al. (2015), and techniques by Frey et al. (2004), Frey and Mende (2006), Liou (2010), the Newell and Gjerloev technique (P. Newell & Gjerloev, 2011), and the Ohtani and Gjerloev technique (Ohtani & Gjerloev, 2020). They also acknowledge the SuperMAG collaboration (Gjerloev, 2012) and the NASA/GSFC's Space Physics Data Facility for providing open-source access to the relevant data. This research received support from NSF Grant 2134451, and the authors extend their thanks to the Department of Electrical and Computer Engineering at the University of South Alabama for their cooperation. The authors express their sincere gratitude to the editors and reviewers for their insightful comments and constructive feedback, which have significantly enhanced the quality of this manuscript.

References

Adhya, P. (2025). Substorm dataset and code (substorm identification with the windmi magnetosphere - Ionosphere nonlinear physics model). *Zenodo*. https://doi.org/10.5281/zenodo.14607257

Akasofu, S.-I. (1964). The development of the auroral substorm. *Planetary and Space Science*, *12*(4), 273–282. https://doi.org/10.1016/0032-0633(64)90151-5

Akasofu, S. I. (1981). Energy coupling between the solar wind and the magnetosphere. *Space Science Reviews*, *28*(2), 121–190. https://doi.org/10.1007/BF00218810

Axford, W. I., & Hines, C. O. (1961). A unifying theory of high-latitude geophysical phenomena and geomagnetic storms. *Canadian Journal of Physics*, *39*(10), 1433–1464. https://doi.org/10.1139/p61-172

Baker, D., Li, X., Turner, N., Allen, J., Bargatze, L., Blake, J., et al. (1997). Recurrent geomagnetic storms and relativistic electron enhancements in the outer magnetosphere: Istp coordinated measurements. *Journal of Geophysical Research: Space Physics*, *102*(A7), 14141–14148. https://doi.org/10.1029/97ja00565

Baker, D., Pulkkinen, T., Buchner, J., & Klimas, A. (1999). Substorms: A global instability of the magnetosphere-ionosphere system. *Journal of Geophysical Research: Space Physics*, *104*(A7), 14601–14611. https://doi.org/10.1029/1999ja900162

Beharrell, M., Honary, F., Rodger, C., & Clilverd, M. (2015). Substorm-induced energetic electron precipitation: Morphology and prediction. *Journal of Geophysical Research: Space Physics*, *120*(4), 2993–3008. https://doi.org/10.1002/2014ja020632

Davis, T. N., & Sugiura, M. (1966). Auroral electrojet activity index ae and its universal time variations. *Journal of Geophysical Research*, *71*(3), 785–801. https://doi.org/10.1029/jz071i003p00785

Ebihara, Y., & Tanaka, T. (2017). Energy flow exciting field-aligned current at substorm expansion onset. *Journal of Geophysical Research: Space Physics*, *122*(12), 12–288. https://doi.org/10.1002/2017ja024294

Ebihara, Y., & Tanaka, T. (2023). Generation of field-aligned currents during substorm expansion: An update. *Journal of Geophysical Research: Space Physics*, *128*(2), e2022JA031011. https://doi.org/10.1029/2022ja031011

Feldstein, Y. I., Grafe, A., Gromova, L., & Popov, V. (1997). Auroral electrojets during geomagnetic storms. *Journal of Geophysical Research: Space Physics*, *102*(A7), 14223–14235. https://doi.org/10.1029/97ja00577

Forsyth, C., Rae, I., Coxon, J., Freeman, M., Jackman, C., Gjerloev, J., & Fazakerley, A. (2015). A new technique for determining substorm onsets and phases from indices of the electrojet (sophie). *Journal of Geophysical Research: Space Physics*, *120*(12), 10–592. https://doi.org/10.1002/2015ja021343

Forsyth, C., Shortt, M., Coxon, J., Rae, I., Freeman, M., Kalmoni, N., et al. (2018). Seasonal and temporal variations of field-aligned currents and ground magnetic deflections during substorms. *Journal of Geophysical Research: Space Physics*, *123*(4), 2696–2713. https://doi.org/10.1002/2017ja025136

Freeman, M., & Morley, S. K. (2004). A minimal substorm model that explains the observed statistical distribution of times between substorms. *Geophysical Research Letters*, *31*(12). https://doi.org/10.1029/2004gl019989

Frey, H., & Mende, S. (2006). Substorm onsets as observed by image-fuv. In *International conference on substorms* (Vol. 8, pp. 71–75).

Frey, H., Mende, S., Angelopoulos, V., & Donovan, E. (2004). Substorm onset observations by image-fuv. *Journal of Geophysical Research: Space Physics*, *109*(A10). https://doi.org/10.1029/2004ja010607

Gjerloev, J. (2012). The supermag data processing technique. *Journal of Geophysical Research: Space Physics*, *117*(A9). https://doi.org/10.1029/2012ja017683

Gjerloev, J., & Hoffman, R. (2002). Currents in auroral substorms. *Journal of Geophysical Research: Space Physics*, *107*(A8). SMP-5. https://doi.org/10.1029/2001ja000194

Gordeev, E., Sergeev, V., Tsyganenko, N., Kuznetsova, M., Rastäetter, L., Raeder, J., et al. (2017). The substorm cycle as reproduced by global MHD models. *Space Weather*, *15*(1), 131–149. https://doi.org/10.1002/2016sw001495

Horton, W., & Doxas, I. (1996). A low-dimensional energy-conserving state space model for substorm dynamics. *Journal of Geophysical Research: Space Physic*, *101*(A12), 27223–27237. https://doi.org/10.1029/96ja01638

Horton, W., & Doxas, I. (1998). A low-dimensional dynamical model for the solar wind driven geotail-ionosphere system. *Journal of Geophysical Research: Space Physics*, *103*(A3), 4561–4572. https://doi.org/10.1029/97ja02417

Johnson, J. R., & Wing, S. (2014). External versus internal triggering of substorms: An information-theoretical approach. *Geophysical Research Letters*, *41*(16), 5748–5754. https://doi.org/10.1002/2014gl060928

Kappenman, J. G. (2001). An introduction to power grid impacts and vulnerabilities from space weather: A review of geomagnetic storms, impacts to ground-based technology systems, and the role of forecasting in risk management of critical systems. *Space Storms and Space Weather Hazards*, 335–361.

Kaufmann, R. L. (1987). Substorm currents: Growth phase and onset. *Journal of Geophysical Research: Space Physics*, *92*(A7), 7471–7486. https://doi.org/10.1029/ja092ia07p07471

Lanzerotti, L. J. (2001). Space weather effects on technologies. *Geophysical Monograph Series*, *125*, 11–22. https://doi.org/10.1029/gm125p0011

Liou, K. (2010). Polar ultraviolet imager observation of auroral breakup. *Journal of Geophysical Research: Space Physics*, *115*(A12). https://doi.org/10.1029/2010ja015578

Liou, K., Newell, P. T., Zhang, Y.-L., & Paxton, L. J. (2013). Statistical comparison of isolated and non-isolated auroral substorms. *Journal of Geophysical Research: Space Physics*, *118*(5), 2466–2477. https://doi.org/10.1002/jgra.50218

Lyons, L. (1996). Substorms: Fundamental observational features, distinction from other disturbances, and external triggering. *Journal of Geophysical Research: Space Physics*, *101*(A6), 13011–13025. https://doi.org/10.1029/95ja01987

Mays, M., Horton, W., Spencer, E., & Kozyra, J. (2009). Real-time predictions of geomagnetic storms and substorms: Use of the solar wind magnetosphere-ionosphere system model. *Space Weather*, *7*(7). https://doi.org/10.1029/2008sw000459

McPherron, R., Terasawa, T., & Nishida, A. (1986). Solar wind triggering of substorm expansion onset. *Journal of Geomagnetism and Geoelectricity*, *38*(11), 1089–1108. https://doi.org/10.5636/jgg.38.1089

McPherron, R. L. (1979). Magnetospheric substorms. *Reviews of Geophysics*, *17*(4), 657–681. https://doi.org/10.1029/rg017i004p00657

Morley, S. K., & Freeman, M. (2007). On the association between northward turnings of the interplanetary magnetic field and substorm onsets. *Geophysical Research Letters*, *34*(8). https://doi.org/10.1029/2006gl028891

Morley, S. K., Freeman, M., & Tanskanen, E. (2007). A comparison of the probability distribution of observed substorm magnitude with that predicted by a minimal substorm model. *Annales Geophysicae*, *25*(11), 2427–2437. https://doi.org/10.5194/angeo-25-2427-2007

Morley, S. K., Rouillard, A., & Freeman, M. P. (2009). Recurrent substorm activity during the passage of a corotating interaction region. *Journal of Atmospheric and Solar-Terrestrial Physics*, *71*(10–11), 1073–1081. https://doi.org/10.1016/j.jastp.2008.11.009

Newell, P., & Gjerloev, J. (2011a). Substorm and magnetosphere characteristic scales inferred from the supermag auroral electrojet indices. *Journal of Geophysical Research: Space Physics*, *116*(A12). https://doi.org/10.1029/2011JA016936

Newell, P. T., & Gjerloev, J. (2011b). Evaluation of supermag auroral electrojet indices as indicators of substorms and auroral power. *Journal of Geophysical Research: Space Physics*, *116*(A12). https://doi.org/10.1029/2011JA016779

Newell, P. T., & Liou, K. (2011). Solar wind driving and substorm triggering. *Journal of Geophysical Research: Space Physics*, *116*(A3). https://doi.org/10.1029/2010ja016139

Ohtani, S., & Gjerloev, J. W. (2020). Is the substorm current wedge an ensemble of wedgelets? Revisit to midlatitude positive bays. *Journal of Geophysical Research: Space Physics*, *125*(9), e2020JA027902. https://doi.org/10.1029/2020ja027902

Rostoker, G., & Fälthammar, C.-G. (1967). Relationship between changes in the interplanetary magnetic field and variations in the magnetic field at the earth's surface. *Journal of Geophysical Research*, *72*(23), 5853–5863. https://doi.org/10.1029/jz072i023p05853

Shukhtina, M., Dmitrieva, N., Popova, N., Sergeev, V., Yahnin, A., & Despirak, I. (2005). Observational evidence of the loading-unloading substorm scheme. *Geophysical Research Letters*, *32*(17). https://doi.org/10.1029/2005gl023779

Spencer, E., Horton, W., Mays, L., Doxas, I., & Kozyra, J. (2007). Analysis of the 3-7 October 2000 and 15-24 April 2002 geomagnetic storms with an optimized nonlinear dynamical model. *Journal of Geophysical Research: Space Physics*, *112*(A04S90). https://doi.org/10.1029/2006JA012019

Spencer, E., Vadepu, S. K., Srinivas, P., Patra, S., & Horton, W. (2018). The dynamics of geomagnetic substorms with the windmi model. *Earth Planets and Space*, *70*, 1–9. https://doi.org/10.1186/s40623-018-0882-9

Weimer, D. (1994). Substorm time constants. *Journal of Geophysical Research: Space Physics*, *99*(A6), 11005–11015. https://doi.org/10.1029/93ja02721

Weimer, D. (2001). An improved model of ionospheric electric potentials including substorm perturbations and application to the geospace environment modeling november 24, 1996, event. *Journal of Geophysical Research: Space Physics*, *106*(A1), 407–416. https://doi.org/10.1029/2000ja000604